Available online at www.sciencedirect.com

ScienceDirect

Biochimica et Biophysica Acta 1768 (2007) 509–520

Biochimica et Biophysica Acta BBA

www.elsevier.com/locate/bbamem

Structure of the antimicrobial β-hairpin peptide protegrin-1 in a DLPC lipid bilayer investigated by molecular dynamics simulation

Himanshu Khandelia [a], Yiannis N. Kaznessis [a,b,*]

[a] Department of Chemical Engineering and Materials Science and University of Minnesota, 421, Washington Avenue SE, Minneapolis, MN 55455, USA
[b] The Digital Technology Center, University of Minnesota, 421, Washington Avenue SE, Minneapolis, MN 55455, USA

Received 26 July 2006; received in revised form 17 November 2006; accepted 21 November 2006
Available online 15 December 2006

Abstract

All atom molecular dynamics simulations of the 18-residue β-hairpin antimicrobial peptide protegrin-1 (PG-1, RGGRLCYCRRRFCVCVGR-NH_2) in a fully hydrated dilauroylphosphatidylcholine (DLPC) lipid bilayer have been implemented. The goal of the reported work is to investigate the structure of the peptide in a membrane environment (previously solved only in solution [R.L. Fahrner, T. Dieckmann, S.S.L. Harwig, R.I. Lehrer, D. Eisenberg, J. Feigon, Solution structure of protegrin-1, a broad-spectrum antimicrobial peptide from porcine leukocytes. Chemistry and Biology, 3 (1996) 543–550]), and to delineate specific peptide–membrane interactions which are responsible for the peptide's membrane binding properties. A novel, previously unknown, "kick" shaped conformation of the peptide was detected, where a bend at the C-terminal β-strand of the peptide caused the peptide backbone at residues 16–18 to extend perpendicular to the β-hairpin plane. This bend was driven by a highly persistent hydrogen-bond between the polar peptide side-chain of TYR7 and the unshielded backbone carbonyl oxygen atom of GLY17. The H-bond formation relieves the unfavorable free energy of insertion of polar groups into the hydrophobic membrane core. PG-1 was anchored to the membrane by strong electrostatic binding of the protonated N-terminus of the peptide to the lipid head group phosphate anions. The orientation of the peptide in the membrane, and its influence on bilayer structural and dynamic properties are in excellent agreement with solid state NMR measurements [S. Yamaguchi, T. Hong, A. Waring, R.I. Lehrer, M. Hong, Solid-State NMR Investigations of Peptide–Lipid Interaction and Orientation of a b-Sheet Antimicrobial Peptide, Protegrin, Biochemistry, 41 (2002) 9852–9862]. Importantly, two simulations which started from different initial orientations of the peptide converged to the same final equilibrium orientation of the peptide relative to the bilayer. The kick-shaped conformation was observed only in one of the two simulations.

1. Introduction

Antimicrobial peptides (AMPs) are small peptides secreted by organisms across the evolutionary spectrum as a first line of defense against external pathogenic attack [3]. The non-specific membrane-mediated mechanism of microbial lysis by AMPs has elicited optimism in their use as potential alternatives to conventional antibiotics, because conventional antibiotics are more liable to becoming ineffective by the development of antibiotic resistance in pathogens [4]. However, there has not been much success in the use of AMPs or AMP derivatives in the clinic, partly because their rational design is hampered by a lack of knowledge of their mechanism of membrane lysis.

Protegrin-1 (PG-1, RGGRL CYCRR RFCVC VGR-NH_2) is an 18-residue β-hairpin antimicrobial peptide which was first isolated from porcine neutrophils in 1993 [5]. PG-1 has very low minimum inhibitory concentration (MIC) values (0.12 to 2.0 μg/ml) against a large variety of microorganisms, including the problematic methycillin-resistant *Staphylococcus aureus* (MRSA) strain [6]. Several studies confirmed that PG-1 lyses bacterial cells by a membrane-mediated mechanism wherein the peptide either has a significant membrane thinning effect [7] or forms stable pores in fully hydrated planar lipid bilayers [8,9]. X-ray diffraction experiments showed that the peptide completely destabilizes monolayers composed of lipid A, a major component of the outer cell membrane of bacterial cells [10]. PG-1 also has a membrane-thinning effect in in-vivo systems [11].

* Corresponding author. Department of Chemical Engineering and Materials Science and University of Minnesota, 421, Washington Avenue SE, Minneapolis, MN 55455, USA. Tel.: +1 612 624 4197; fax: +1 612 626 7246.
E-mail addresses: hkhandel@cems.umn.edu (H. Khandelia), yiannis@cems.umn.edu (Y.N. Kaznessis).

0005-2736/$ - see front matter © 2006 Elsevier B.V. All rights reserved.
doi:10.1016/j.bbamem.2006.11.015

Unlike helical AMPs, most of which adopt a helical conformation only near membranes or in membrane-like media, PG-1 has a well-defined β-hairpin conformation even in aqueous solution [1,12], owing to the presence of two disulfide linkages which stabilize peptide structure. Removal of the disulfide bridges reduces the antimicrobial potency of PG-1 significantly [11,13,14]. The antimicrobial efficacy of PG-1 is retained at physiological salt concentrations [11], because the peptide is structurally robust in aqueous media. Furthermore, a disulfide-linked structure simplifies the characterization of PG-1 in membranes. The stable structure of PG-1 and its low MIC against a large variety of microorganisms led to considerable excitement about its use for clinical purposes, particularly for the treatment of cystic fibrosis [15] and oral mucositis [14,16]. However, attempts to synthesize novel protegrin antimicrobials have not succeeded beyond phase II trials [17].

Knowledge of the membrane-lytic activity of PG-1 triggered several investigations for determining the membrane-bound state and orientation of the peptide mostly in planar lipid bilayers of varying compositions [2,7–9,18–28]. Solid state NMR experiments show that PG-1 destroys the orientational order of palmitoyloleoylphosphatidylcholine (POPC) lipid bilayers, but does not have so drastic an impact on shorter chain dilauroylphosphatidylcholine (DLPC) lipid bilayers [2]. The peptide has a transmembrane, tilted orientation in DLPC lipid bilayers. Local thinning of the DLPC bilayer owing to hydrophobic mismatch phenomenon was also suggested [21]. In 2003, Buffy et al. [22] showed for the first time that PG-1 forms oligomeric aggregates in POPC bilayers. The oligomeric, immobilized state of PG-1 in POPC was further confirmed by ^{19}F spin diffusion NMR experiments [20,28]. The peptide also forms small nanometer sized aggregates in phosphate buffer saline [27]. Interestingly, no dimers were observed in DLPC lipid bilayers.

Despite the spate of investigations into the mechanism of action of PG-1, some key questions remain unanswered. Although the solution structure of PG-1 was reported in 1996 [1,29], the structure of the peptide in lipid bilayers has not been solved (while this manuscript was being written, the dimer structure of PG-1 in POPC bilayers was published [28]). Because it is stabilized by two disulfide linkages, it is unlikely that there would be large-scale differences in the core of the structure of PG-1 (residues 4–15) in membranes versus in solution. However, it is possible that the peptide may undergo conformational changes at the free C-terminus (residues 16–18) and the N-terminus (residues 1–3). There is also a distinct possibility that the length of the peptide backbone may adjust to the hydrophobic thickness of the lipid bilayer. Molecular dynamics simulations can provide the detailed molecular description of the influence of the lipid bilayer amphipathic environment on the structure of PG-1. Simulations can also quantitatively characterize specific intra-peptide, peptide–lipid, and peptide–water interactions that determine the tilted orientation of PG-1 in the DLPC bilayer. The current work is also a first step towards investigating more complex phenomena such as PG-1 oligomerization in membranes [20], and its selectivity towards longer chain lipids [25] or towards anionic lipids in preference to zwitterionic lipids [8,10].

There is some debate in the literature about the use of the correct thermodynamic ensemble to simulate interfacial systems like lipid bilayers. The debate mainly arises from the question of whether or not real lipid bilayers or bilayer vesicles have a non-vanishing surface tension at the lipid–water interface [30–32]. Although the constant pressure constant temperature (*NPT*) ensemble is commonly used to allow the surface area of the lipid bilayer to relax in response to perturbations like peptide insertion, these simulations often run into area-per-lipid equilibration problems for most lipid types, especially for CHARMM [33], one of the most commonly used force fields. In CHARMM [34], the NP_ZAT or the $NP\gamma T$ ensembles have been recommended for interfacial systems [35,36]. In the former ensemble, the area per lipid is kept fixed, but the simulation cell is free to fluctuate in the direction of the bilayer normal. In the latter, simulations are carried out at a constant surface tension. We have used the NP_ZAT ensemble in the current work, because an accurate area per lipid value is available for the DLPC bilayer. The simulation with the peptide starts off with the peptide in a transmembrane orientation, and it is assumed that changes in the area of the bilayer as a result of peptide reorientation are small enough to avoid artifacts arising from incorrect pressure profiles.

2. Methods

Molecular dynamics simulations of a single PG-1 peptide in a DLPC lipid bilayer were implemented. Simulation of a pure hydrated DLPC bilayer was carried out first. The CHARMM27 force field was used for the simulations. The parameters and topology of the DLPC lipid were obtained by reducing the 14-carbon fatty acid chains of the DMPC lipid to 12-carbon fatty acid chains. The topology and parameters of the DMPC lipid are available in the CHARMM force field.

The initial coordinates of the DLPC lipid bilayer were built using the methodology suggested in the CHARMM support documents [37]. Each lipid leaflet contained 64 lipids, with the fatty acid chains of both leaflets pointing towards each other towards the center of the simulation cell. Each leaflet of the bilayer was hydrated by an approximately 20 Å thick layer of water, which was modeled by a TIP3P potential [38]. The assembly was placed in a triclinic simulation cell, defined by the coordinate system *XYZ*, with the *Z* axis along the bilayer normal. The ratio of the cell dimensions in the plane of the bilayer (*X*:*Y*) was kept at 1:1 at all times. The lateral (*XY*) dimensions of the simulation cell were determined as described below.

2.1. Determination of simulation cell dimensions

Determination of the cell dimensions in the bilayer plane is a critical step in the construction of an accurate model of a lipid bilayer, because the cell dimensions determine the area per lipid of the membrane, (a quantity that can be accurately measured from X-ray diffraction experiments), and has a significant impact on simulation results. Use of an incorrect area per lipid leads to an incorrect lipid density and can thus result in severe simulation artifacts. To specify the correct simulation cell size, either the area per lipid needs to be known a-priori, or a constant pressure, constant temperature (*NPT*) ensemble must be used for the area to relax to its equilibrium value. Because the area per lipid for the DLPC lipid bilayer has been estimated from X-ray diffraction experiments [39–41], we used the NP_ZAT ensemble to run the simulations. To ensure that the right initial pressure profile was obtained, the simulation cell was assigned initial dimensions such that the area per lipid was larger than the expected equilibrium value. In this state, a short simulation was run in the *NPT*

ensemble (P = 1 atmosphere), wherein the system was allowed to relax until the area per lipid shrank to the correct equilibrium value, at which point the simulation was stopped. The final set of coordinates obtained from this simulation was used to start a new simulation in the NP_ZAT ensemble. This procedure ensures that the correct area per lipid is used in the NP_ZAT simulation, while avoiding possible artifacts from incorrect pressure profiles. The area per lipid of the DLPC lipid bilayer in the liquid crystalline phase has been independently reported by various investigators [39–41] at temperatures ranging from 20° to 30 °C. The simulations in the current work were run at 40 °C for faster dynamics. The area per lipid at 40 °C was obtained by using a linear coefficient of areal expansion of 0.005 per degree [39]. The average value obtained for the area per lipid was 66.8 Å^2, the average of the values suggested from different experiments [39–41].

2.2. Simulation parameters

150 mM NaCl (17 sodium and 17 chloride ions) was added to the bulk phase in all simulations to mimic physiological salt concentrations. For simulations of the pure lipid bilayer, the lipids and the bulk phase (water and ions) were subjected to weak harmonic constraints with spring constants of 10 and 5 kcal/mol Å respectively. These constraints were gradually decreased as the system was subject to steepest descent minimization for ~75 000 steps. Thereafter, the hydrated bilayer assembly was gradually heated to a temperature of 313.15 K. Subsequently the hydrated lipid–water–ion assembly of about 37 000 atoms was subjected to NP_ZAT dynamics using the leap-frog integrator in CHARMM [34]. A time step of 2 fs was used. The temperature was set at 313.15 K using Nose–Hoover temperature control [42]. For the extended system pressure algorithm employed, the X and Y components of the piston mass array were set to zero to fix the area of the bilayer, while the Z component was set to 500 amu [43]. The electrostatic interactions were simulated using the particle mesh Ewald (PME) summation [44] without truncation and a real space Gaussian width of 0.25 Å^{-1}, a β-spline order of 4, and a FFT grid of about one point per Å. The non-bonded van der Waals interactions were smoothly switched off over a distance of 3.0 Å, between 9 Å and 12 Å. SHAKE was used to eliminate the fastest degrees of freedom involving bonds with hydrogen atoms. The simulations were carried out using CHARMM version c30b2 with the all atom param27 parameter set. Image lists were updated every 25 steps, and coordinates were saved every 10 ps. The initial setup of the simulation has been rendered in Fig. 1A.

2.3. Simulations with the peptide

The coordinates of the PG-1 peptide were obtained from solution structure [1] of PG-1 available in the PDB databank (PDB ID 1PG1). Solid-state NMR experiments suggest that PG-1 has a transmembrane orientation in DLPC lipid bilayers [2,21]. To eliminate conformational bias in the simulations, we placed the peptide in two different starting orientations in the bilayer. In one conformation (CONF1), the peptide was placed with its principal axis parallel to the bilayer normal (Fig. 1C). In the other conformation (CONF2), it was placed at 45° to the bilayer normal (Fig. 1E). In either case, the peptide had a transmembrane orientation. The surface area occupied by the peptide was estimated using the programs available in the CHARMM membrane module, and was found to be 160 Å^2. This area was calculated for the experimentally measured orientation of the peptide: at 45° to the bilayer normal. Two lipids in each leaflet which were closest to the backbone of the peptide were deleted. The total surface area of the bilayer–peptide system was estimated by adding the surface area of the peptide to the surface area of the remaining 62 lipids in each leaflet. Initial bad contacts between the peptide and the lipids were removed by keeping the backbone of the peptide constrained during the minimization phase of the simulations. Thereafter, the simulations were run in a similar fashion as the simulations of the pure bilayers as described above, including the NPT phase where the area was equilibrated initially. The peptide was amidated at the C-terminus, and protonated at the N-terminus, and had 6 cationic arginine residues. Therefore, 7 chloride counterions were randomly distributed in the bulk phase to set the total charge of the system to zero. All quantities, other than the orientation of the peptide (which changed during the initial NPT part of the simulation), were calculated from the NP_ZAT part of the simulations.

3. Results: pure bilayer simulation

3.1. Structure of the pure lipid bilayer

The focus of the current article is on lipid–peptide interactions. We will only briefly discuss the structural and dynamic properties of the lipid bilayer, to justify the methods used. The simulation of the pure lipid bilayer was carried out for 20 ns, and ensemble averages were drawn for the last 12 ns of simulation.

The overall electron density profiles in the simulations and the experiments [39] are compared in Fig. 2B and are very similar. In Fig. 2A, the individual profiles for the electron density have been constructed. The average distance between the maxima in the profile (head–head distance) is 30.4 Å, which is close to the reported value for the average head–head distance is 30.8 Å at 30 °C [39]. The average phosphate–phosphate distance was ~30 Å. The average mean positions of the electron density peaks of the glycerol backbone, as well as of the choline region of the head group are in excellent agreement with X-ray measurements [39], except that the width of the Gaussian density distributions in the simulations is slightly greater, because of more fluctuations at the higher temperature.

3.2. Order parameter

The dynamics and structural characteristics of the hydrocarbon interior of the lipid bilayer are routinely characterized by the order parameter [37]. In Fig. 3, the average order parameters for both sn1 and sn2 lipid chains are shown. We did not find any experimental measurements for the order parameters of the DLPC bilayer in literature to compare our results with. However, the experimentally estimated order parameters for a DMPC bilayer at 40 °C [45] are shown in Fig. 3 for comparison. The general shape of the order parameter curve, as well as the expected numbers at each hydrocarbon position are comparable to experimental measurements.

It is clear that the constant area ensemble used in the current work accurately reproduces both the structure (electron density) and the dynamics (orientational order parameters) of the bilayer accurately.

4. Results: peptide-bilayer simulation

4.1. Peptide orientation in the bilayer

The complete description of the orientation of the β-hairpin peptide in the DLPC lipid bilayer requires the definition of two angles: the tilt of the peptide from the bilayer normal (τ) and the angle of rotation between the bilayer normal and the normal to the plane of the peptide (φ) (Fig. 4) [2]. The angle τ was calculated by measuring the angle between bilayer normal and the unit vector of the principal axis of the moment of inertia of the backbone atoms of the peptide. The angle of rotation φ was calculated by measuring the angle between the bilayer normal and the normal to the least squared plane formed by the peptide

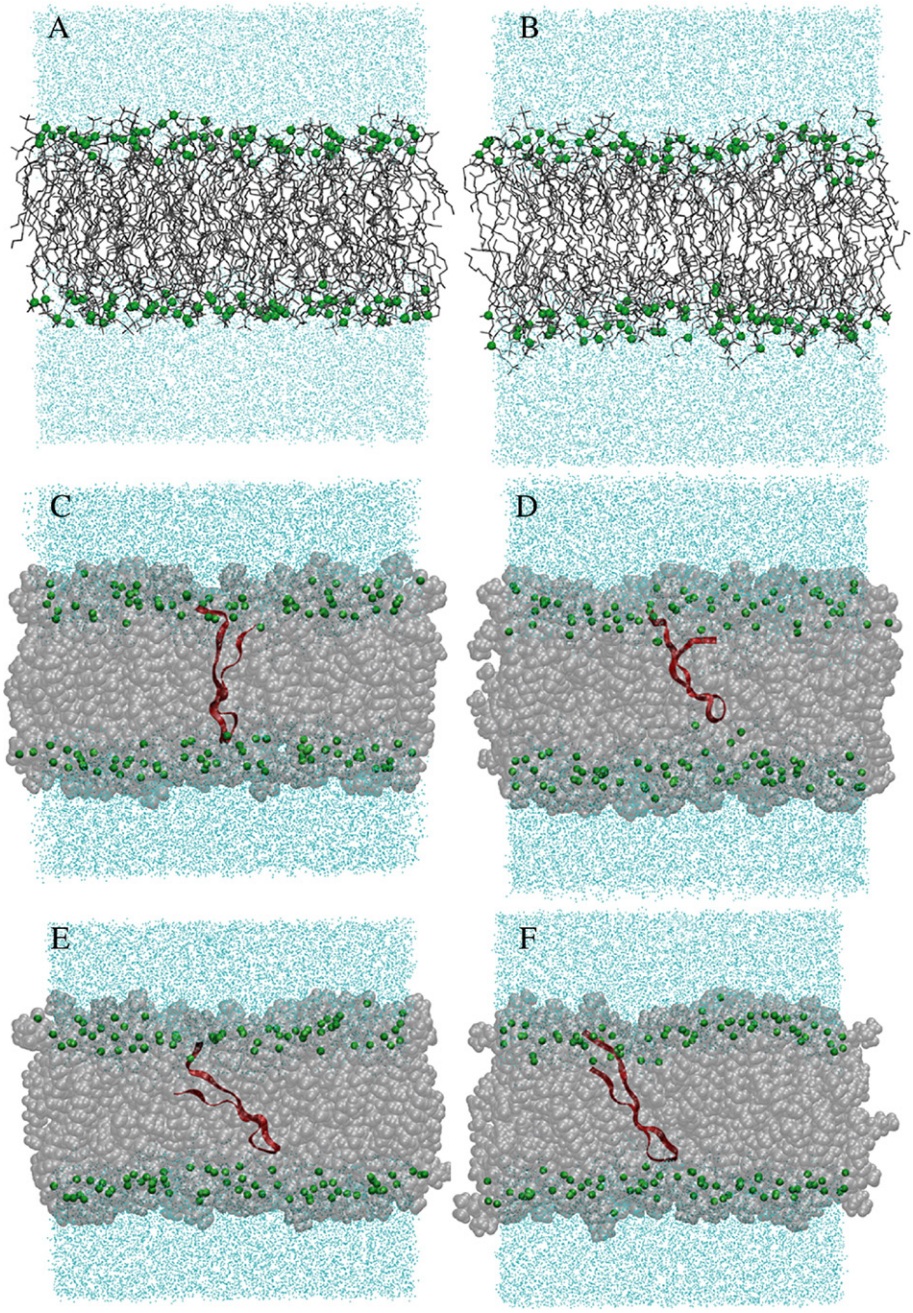

Fig. 1. (A and B) Initial and final (t=20 ns) snapshots of the pure bilayer simulation. (C and D) Initial and final (t=24 ns) snapshots of the CONF1 peptide-bilayer simulation. (E and F) Initial and final (t=24 ns) snapshots of the CONF2 peptide-bilayer simulation. In each case, the area per lipid in the initial setup was set larger than the expected equilibrium value.

backbone. Both simulations CONF1 and CONF2 converged to similar values of the angles τ and φ (Fig. 5). All ensemble averages for the simulations were drawn after 10 ns, when both the angle of rotation φ and the tilt angle τ had converged. Solid state NMR experiments were used by Yamaguchi et al. [2] to determine the orientation of PG-1 in DLPC bilayers. The analysis therein required the coordinates from the deposited solution structures of PG-1 in the pdb data bank. Using five of the twenty available structures, analysis of chemical shifts yielded tilt angles ranging from 50° to 73°. If data are combined from simulations CONF1 and CONF2, then the maximum and minimum values of τ are 37° and 75°. However, on an average, the simulations yield τ values ranging between approximately 42° and 72°, which are fairly close to the experimentally calculated orientation angles. The range of angles accessible to the simulations is larger because the peptide can adopt a larger variety of conformations. In NMR, the range of 50°–73° was obtained using only five solution structures in calculations.

The angle of rotation φ was only calculated for a single PG-1 structure using NMR, and the reported value was 48°±5°. Although these values of φ are often sampled in the simulations

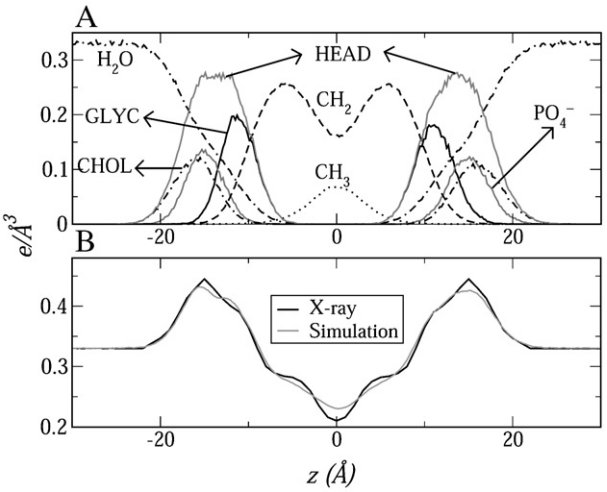

Fig. 2. (A) Ensemble averaged electron density in the pure lipid bilayer simulation. The bulk electron density was 0.33 electrons/Å^3. CHOL: choline group. PO_4^-: Phosphate anions. GLYC: Glycerol backbone. HEAD: Sum of CHOL, PO_4^- and GLYC. CH_2: Fatty acid methylene groups. CH_3: Terminal methyl groups. (B) Comparison of the total electron density in the simulation to the experimental results of Kucerka et al. [39]. A 10-point average was used to smooth the simulation curve.

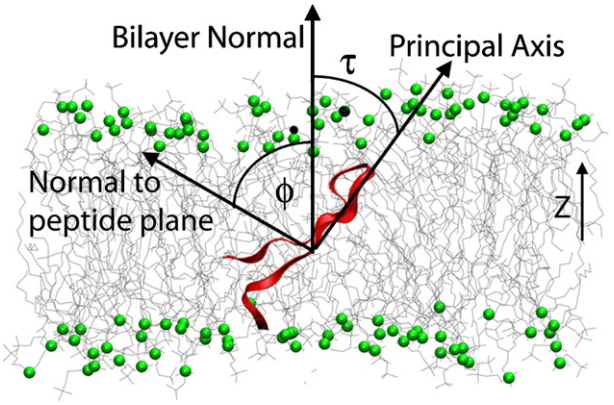

Fig. 4. Schematic description of the tilt angle τ and the angle of rotation φ. Adapted from Yamaguchi et al. with permission [2].

(Fig. 5), the average φ observed in the simulations is nearly 60°. The slight discrepancy can again be attributed to the incomplete sampling of conformations in the calculation of angles in the NMR experiments.

4.2. Peptide structure

The overall root mean squared deviation (rmsd) of the peptide backbone converged to steady state values of 2.5 Å and 2.0 Å in the CONF1 and CONF2 simulations respectively. The steady state backbone dihedral angle values for the core of the peptide (residues 4–15) were similar in both simulations and indicate a β-hairpin structure. Most of the figures constructed from here on will pertain to the CONF1 simulation. Results from the CONF2 simulations will be confined to discussion in the text.

A clustering algorithm of peptide backbone dihedral angles was implemented to detect distinct peptide conformations in the production period. Time series of the peptide dihedral angles were obtained from different initial timepoints t_{ini} in the trajectory. t_{ini} was varied from $t_{ini}=0$ ns to $t_{ini}=20.0$ ns with a 2 ns interval. Thus, each set of time series contained the dihedral

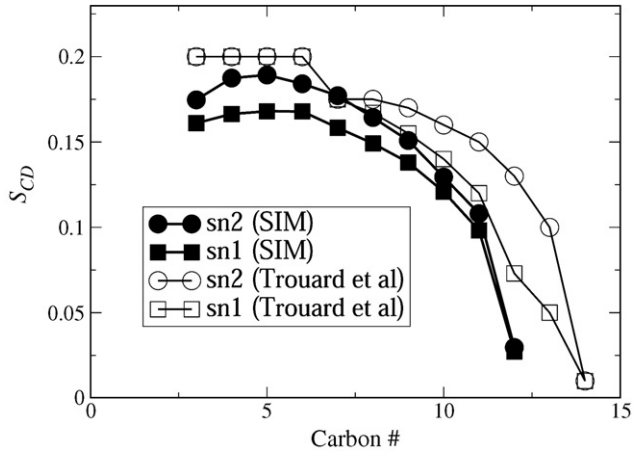

Fig. 3. Order parameters (S_{CD}) of the DLPC lipid bilayer calculated from the simulations, compared to the experimental measurements of the order parameters of a DMPC lipid bilayer [45]. Experimental estimates of S_{CD} for DLPC bilayers were not available in literature.

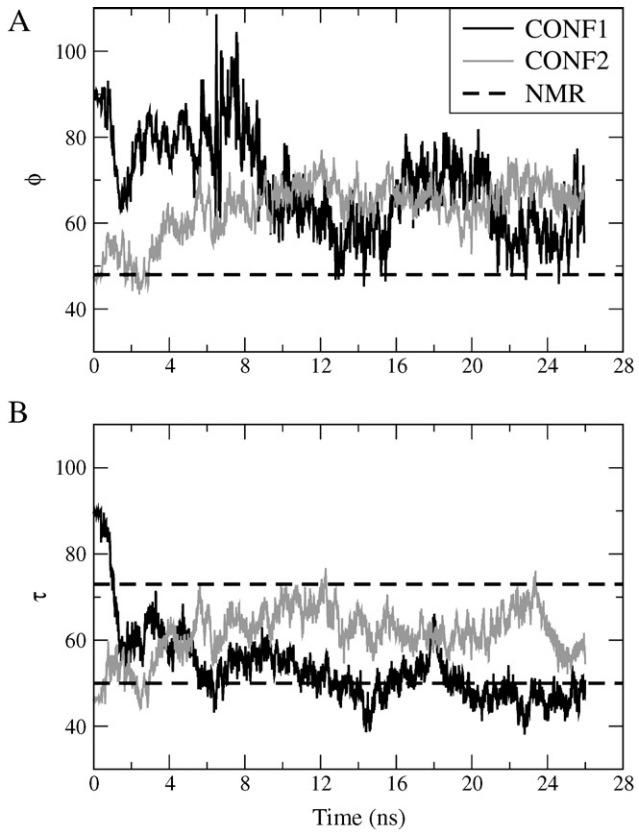

Fig. 5. Time profiles for the angle of rotation (φ) (A) and the angle of tilt (τ) (B) of PG-1. The range of NMR estimates for τ has been shown as parallel dashed lines in B. For φ, only one NMR estimate was made, shown as a dashed line in panel A.

angle values for the peptide for a trajectory window starting at time t_{ini}, till the end of the simulation. Each set of time series was clustered using the ART-2 clustering algorithm in CHARMM. The number of clusters thus obtained is a good measure of the number of different peptide conformations sampled during a trajectory window. Cluster radii of 25, 30 and 35 resulted in detection of 3, 2 and 1 peptide conformations, respectively. However, when the clustering was carried out for the residues 3–15, only one equilibrium conformation was detected at for all three clustering radii, thus indicating that the greater number of peptide conformations arose from the fluctuation of the free peptide termini, and that there was only one stable backbone conformation in the simulation.

In Fig 6, the average dihedral angles of the peptide backbone (φ, ψ) from the CONF1 simulation are compared to the dihedral angles of one of the solved solution structures of PG-1 which was used to start the simulation. The peptide consists of two antiparallel β-strands stretching from residues 4–9 and 12–15 separated by a β-turn at residues 9–11. The peptide conformations from the simulations are similar to those obtained in solution by Fahrner et al. [1] for the core of the peptide (residues 4–15). Aumelas and coworkers [29] had calculated the β-strands to extend from positions 5–9 and 12–16. The position of the turn is exactly the same in both the independent investigations of the solution structure [1,29] and the structure in the lipid bilayer simulations. A similar structure was obtained in the CONF2 simulation for residues 3–15.

A detailed H-bonding analysis was carried out to describe peptide structure and peptide–lipid interactions. Hydrogen bonds were characterized by a distance and angle-based criterion: all donor–hydrogen acceptor pairs within 2.8 Å of each other and with a donor–hydrogen–acceptor angle of greater than 120° were counted as H-bonding pairs. Trajectories were sampled every 10 ps, and the persistence of each H-bond was measured in terms of the occupancy, which was defined as the ratio between the total observed lifetime of occurrence of the

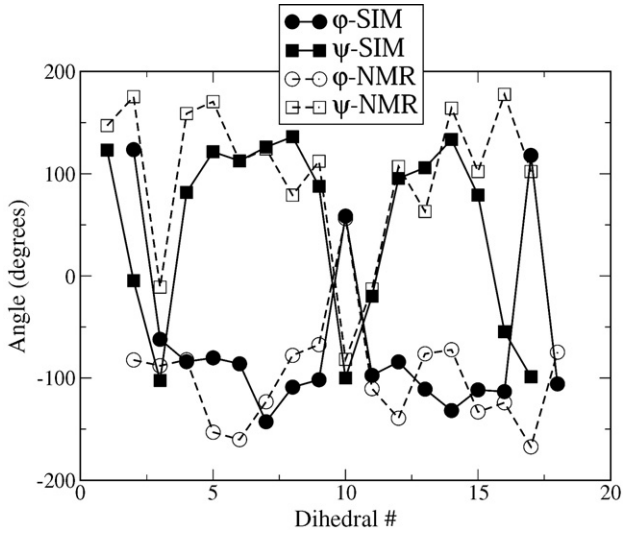

Fig. 6. Average backbone dihedral angles φ and ψ from the simulations compared to the dihedral angles of solution structure of the peptide which was used to start the simulations.

Table 1
H-bonding pairs in the CONF1 simulation

ATOM A			ATOM B			OCC	<TIME>
Backbone-Backbone							
LEU	5	HN	VAL	16	O	0.17	42.8
LEU	5	O	VAL	16	HN	0.15	29.1
TYR	7	HN	VAL	14	O	0.53	50.3
TYR	7	O	VAL	14	HN	0.35	35.4
ARG	9	HN	PHE	12	O	**0.98**	**1016.7**
ARG	9	O	PHE	12	HN	**0.94**	**334.9**
Backbone-Sidechain							
CYS	15	O	ARG	4	HE	0.61	273.6
GLY	17	O	TYR	7	HH	**0.96**	**2384**
Backbone-DLPC							
GLY	2	HN	DLPC	116	O14	0.23	113.2
GLY	3	HN	DLPC	69	O22	0.6	84.6
ARG	4	HN	DLPC	69	O13	0.22	21.4
ARG	4	HN	DLPC	69	O11	0.79	99.6
CYS	6	HN	DLPC	69	O32	0.29	89.2
ARG	10	HN	DLPC	7	O32	0.24	126.2
ARG	11	HN	DLPC	53	O32	0.91	232
PHE	12	HN	DLPC	53	O32	0.26	19.2
CYS	15	HN	DLPC	80	O32	0.9	360.6
Sidechain-DLPC							
ARG	1	HE	DLPC	116	O13	0.42	77.4
ARG	1	HE	DLPC	116	O14	0.22	59.1
ARG	10	HE	DLPC	7	O13	0.3	155.8
ARG	10	HE	DLPC	7	O14	0.3	44
ARG	11	HE	DLPC	53	O13	0.57	141
ARG	11	HE	DLPC	53	O14	0.33	67.7
ARG	18	HE	DLPC	117	O13	0.77	353.3
N-term-DLPC							
ARG	1	HT1	DLPC	113	O14	0.42	178.6
ARG	1	HT1	DLPC	115	O13	0.49	378.1
ARG	1	HT1	DLPC	115	O12	0.15	17.2
ARG	1	HT2	DLPC	113	O14	0.19	45.7
ARG	1	HT3	DLPC	113	O14	0.45	297.9
ARG	1	HT3	DLPC	115	O13	0.41	183.2

Each atom of the pair is described by the residue type, residue number in the sequence, and atom type. OCC is the occupancy of each H-bonding pair, and <TIME> is the average lifetime in ps. The atoms types are as follows: HN: H atom of backbone amide; O: O atom of backbone carbonyl; O1*: O atoms on phosphate groups of lipids; O2* and O3*: O atoms of lipid fatty acid carboxyl groups; HT*: H-atoms of protonated N-terminus.

H-bond and the total time for which the H-bonding analysis was done. In Table 1, the occupancies of H-bonds between the carboxyl oxygen (O) atoms and amide hydrogen (HN) atoms of the peptide are summarized. All H-bonding pairs with occupancy of less than 0.15 were removed from the analysis. Additionally, (*i,i+2*) H-bonds were also eliminated, because they arise from the proximity of residue *i* to residue *i+2* in the peptide sequence. The amide hydrogen (HN) and the carbonyl oxygen (O) atoms of the amino acid residues 5, 7 and 9 on the first β-strand make H-bond bridges with the O and HN atoms of residues 16, 14 and 12 respectively on the second, antiparallel β-strand. In addition to the three H-bonding pairs, the two disulfide bridges formed by the residue pairs of 8–13 and 6–15 stabilize the antiparallel β-hairpin structure. The β-turn at residues 9 through 12 is clearly identified by the nearly 100%

occupancy of the ARG9–PHE12 backbone H-bond. The H-bonding patterns were similar for the CONF2 simulations, including the occurrence of the very well-defined ARG9–PHE12 backbone H-bond. The occupancies of the 5–16 and 7–14 H-bonds were slightly lower for the CONF2 simulations, compared to the CONF1 simulations.

The overall shape of the core of the peptide (residues 4–15) is similar in the solution structure and the simulations. However, the C-terminal residues of the peptide adopted a very different conformation in the lipid bilayer. In the CONF1 simulation, the peptide backbone of residues 16–18 was nearly perpendicular to the plane of the β-hairpin, resulting in what we call a "kick" shaped structure of the peptide (Fig. 7), where one of the two free termini of the peptide is bent away from the backbone. The change in shape was brought about by the formation of an exceptionally strong and persistent H-bond between the hydroxyl group of TYR7 and the backbone O atom of GLY17 (Table 1, Fig. 8). The occupancy of this H-bond was nearly 100%, and the bond was broken only 5 times during the ensemble-averaging period. The C-terminus of the peptide bent back into the bilayer as a result of this H-bond, instead of extending into the interface and the aqueous phase. The tyrosine side chain extended towards the direction of the C-terminus, and a H-bond with GLY17 was formed (and not with VAL16 or ARG18) because the GLY17 backbone is sterically the most accessible, and was not involved in backbone–backbone H-bonds. The peptide adopts the kick conformation from 1.5 ns till the end of the simulation.

The backbone O atom of CYS15 did not form H-bonds with any other backbone HN atom. However, the ARG4 side chain made intermittent H-bonds with the CYS15 backbone (Fig. 8).

The average end-to-end length of the peptide backbone in the CONF1 simulation, based on point coordinates was 25.9±0.67 Å. The average length of the 20 deposited solution structures (PDB ID 1PG1) is 26.3±2.7 Å. The two values are similar despite the kick shaped conformation, because in solution, the N-terminus and the C-terminus of the peptide are free to fluctuate in space, while the N-terminal leg of the peptide is still fully extended in the simulation, and strongly bound to the lipid bilayer (see later). For the CONF2 simulation, the length of the peptide was 28.8±2.0 Å, which is longer than the solution structure because the termini are relatively constrained, and is longer than the CONF1 simulation because of the absence of the kick-shaped conformation.

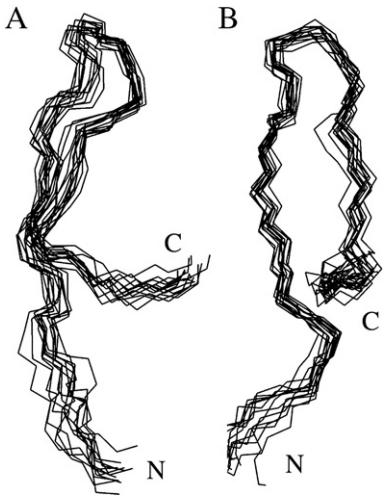

Fig. 7. The "kick"-shaped conformation of the PG-1. The peptide backbones from 10 simulation snapshots from the last 10 ns of the CONF1 simulation were aligned. The C-terminus and N-terminus are marked C and N respectively. A and B are front-end and side-on views.

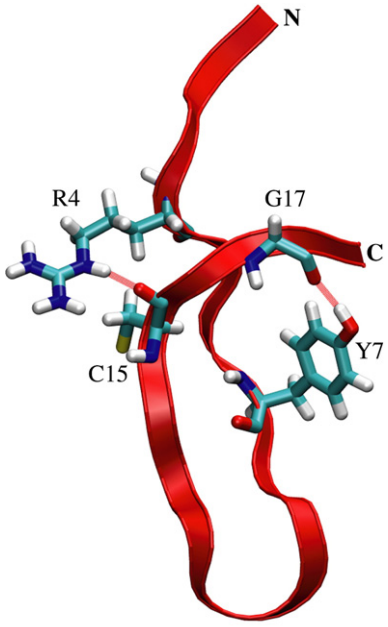

Fig. 8. Simulation snapshot depicting the sidechain-backbone H-bonds between TYR7–GLY17 and ARG4–CYS15. The peptide has been shown as a red ribbon. The C-terminus and N-terminus are marked C and N respectively, and the H-bonds have been depicted by red lines. (For interpretation of the references to colour in this figure legend, the reader is referred to the web version of this article.)

4.3. Peptide–lipid interactions

The β-hairpin structure of PG-1 in the bilayer is distinctly amphipathic. The charged arginine residues populate the termini and the β-turn of the peptide, thus being in close proximity to the membrane interface. The hydrophobic side chains of LEU5, TYR7, PHE12, VAL14 and VAL16 comprise the central hydrophobic region of the peptide, and are inserted into the bilayer core. To delineate specific peptide lipid interactions, we constructed radial distribution functions (RDFS) of the peptide side chains with the hydrophobic core of the bilayer, as well as with the head groups. All RDFS were normalized by the number of atoms in the first selection (which was usually the heavy atoms on the peptide side chain).

4.3.1. N-terminus

The N-terminus of PG-1 is protonated, and thus positively charged. As observed, it was not the arginine residues, but the protonated N-terminus of the peptide which anchored the peptide to the bilayer. Fig. 9 shows the radial distribution

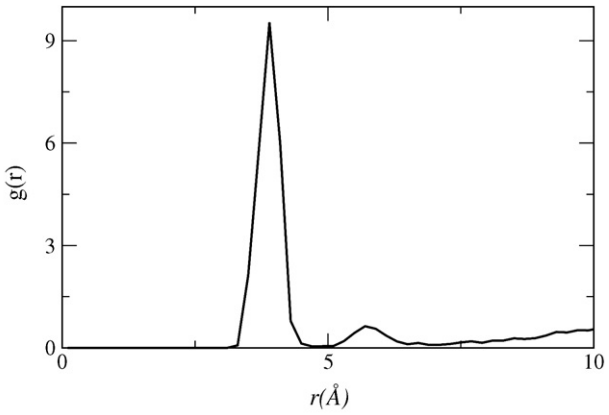

Fig. 9. Radial distribution function between the N-terminal amide nitrogen atom and the phosphorus atoms on two specific lipids which were closest to the N-terminus.

function between the phosphorus atoms of the lipids and the N-terminal amide nitrogen atom. The persistent electrostatic binding of the N-terminus to the lipid head groups anchored the peptide to the lower leaflet of the lipid bilayer. A distance matrix analysis revealed that phosphate anions on two lipid molecules in the lower leaflet remained bound to the N-terminus at all times during the ensemble averaged simulation period. The ensemble averaged probability distribution of the peptide relative to the distribution of the phosphate groups (Fig. 10) shows that the peptide center of mass did not coincide with the bilayer center of mass. Instead, the peptide diffused from the center of the bilayer towards the direction of the lower leaflet head groups, where the two termini of the peptide are localized. The N-terminal peptide anchor resulted in the N-terminus being closer to the interface than the turn region of the peptide. The simulation results explain the experimental measurements of the greater depth of insertion of the β-turn residue PHE12 in comparison to the N-terminal residue GLY2. In the simulation, the C-terminal residues which constitute the "kicking leg" of the peptide were closer to the center of the bilayer, compared to the three N-terminal residues, which constitute the standing leg. The N-terminus did not anchor the peptide to the lipid bilayer in the CONF2 simulation. In CONF1, it is unlikely that the N-terminus anchor is an artifact of the initial conformation, because the N-terminus is initially at a distance of 13.1 Å and 15.4 Å from the two lipids it eventually anchors to.

4.3.2. Arginine residues

The β-turn and the two termini of the peptide are spatially close to the lipid head groups in the trans-membrane orientation of the peptide, and there is a possibility of H-bonding and/or electrostatic interactions between the peptide side chains and either the carboxyl oxygen atoms or the phosphate oxygen atoms on the lipid head groups. In Fig. 11, the radial distribution functions between the peptide side chains and the phosphorus atoms of the lipids have been shown. All the arginine side chains have peaks at 3.8 Å indicating similar types of electrostatic interactions with the phosphate anions. Specifically, ARG10 and ARG18 which are located at spatially opposite ends of the peptide bind most strongly to the phosphates. H-bonds with occupancies greater than 0.5 were formed between the phosphates and the side chains of ARG1, ARG10, ARG11, and ARG18 (Table 1). These H-bonding/electrostatic interactions between the arginine side chains and the lipids are likely to stabilize the trans-membrane orientation of the peptide in the lipid bilayer. The side chain of ARG4 was embedded relatively deeper in the bilayer, and did not form H-bonds with the lipid phosphate groups. The hydroxyl group of TYR7 was not detected to form any persistent H-bond with either water or the lipid head groups, because it formed a stable H-bond with the backbone oxygen atom of GLY17. While ARG1, ARG9, ARG10, ARG11 and ARG18 are all adequately close to the interface to reach out for the phosphate groups, the side chain of ARG4 is relatively deeper in the bilayer, and cannot access the negatively charged phosphate groups of the lipids. RDFS drawn between the peptide side chains and the lipid carboxyl groups revealed that the ARG4 side chain bound electrostatically to the carboxyl oxygen atoms of the sn1 chains of the lipids (data now shown). The sn1 carboxyl groups are slightly closer to the center

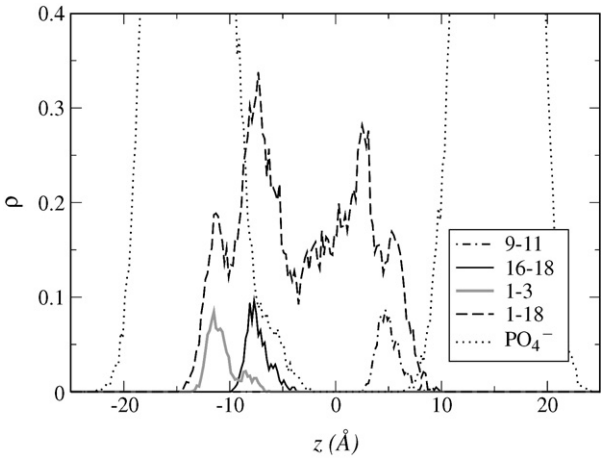

Fig. 10. Probability distribution of the peptide and specific residue regions along the bilayer normal.

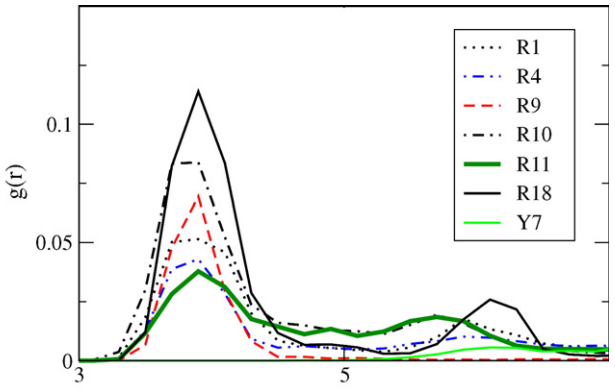

Fig. 11. Radial distribution functions ($g(r)$) between the peptide side chains and the phosphorus atoms on the lipids. The $g(r)$ was normalized by the number of atoms in the first selection, and a random bulk density of 0.01.

of the bilayer than the sn2 carboxyl groups, and are thus more accessible to the ARG4 side chain.

In the CONF2 simulation, the ARG–phosphate interactions were similar except that the ARG4 side chain also formed stronger H-bonds with the phosphate groups.

4.4. Bilayer thickness

The thickness of the lipid bilayer as a function of the distance from the center of mass of the peptide backbone is shown in Fig. 12. The overall phosphate-to-phosphate thickness was obtained by calculating the difference in the average z-coordinate of the phosphate groups located in concentric shells at increasing distance from the center of mass of the peptide backbone. We also calculated the average z-coordinate of the phosphate groups located in concentric shells at increasing distance from the β-turn residues (in the upper leaflet) and the termini residues (in the lower leaflet). The average thickness of the bilayer within 10 Å of the center of mass of the peptide is 23.5 Å, which is about 6 Å smaller than the thickness far away from the peptide. Thus, significant thinning of the lipid bilayer is observed in the simulation. Local thinning of 8–10 Å was predicted in NMR experiments [2]. The discrepancy between the simulations and the experiments is apparently because of the small lipid bilayer size being simulated. Note that the thickness profile calculated from the concentric binning procedure described above has a minimum at the bin 10 Å from the peptide. This bin contains only a single lipid in the lower leaflet, which is strongly H-bonded to ARG18, resulting in the phosphate head group being pulled towards the hydrophobic core, leading to a sharp decrease in thickness 10 Å away from the peptide. Local thinning of the bilayer also resulted in a wider distribution of the phosphate groups, especially in the lower bilayer leaflet (data not shown). Interestingly, in the CONF2 simulation, there was only a slight thinning of the bilayer (~3 Å), even close to the peptide. The reasoning for the differences in the extent of bilayer thinning the CONF1 and CONF2 is discussed later.

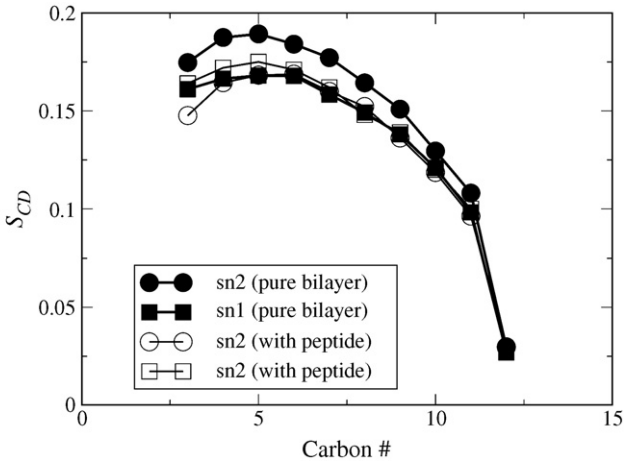

Fig. 12. Bilayer thickness (phosphate-to-phosphate distance) as a function of the distance from the center of mass of the peptide. The average Z coordinate of the upper and lower leaflet have also been shown as a function of the distance from the β-turn and the peptide termini respectively.

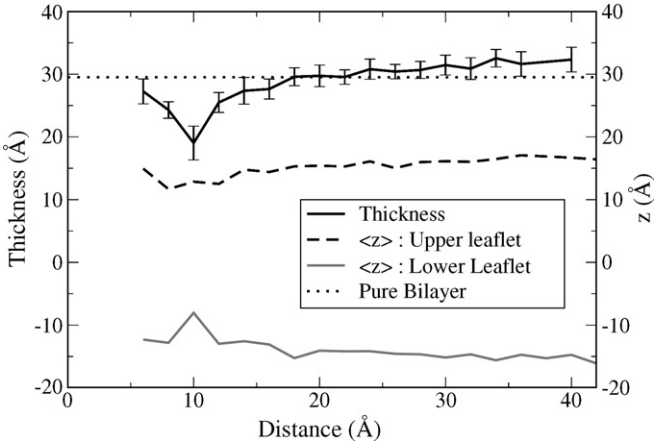

Fig. 13. Average lipid order parameters in the CONF1 simulation compared to the average lipid order parameters from the pure bilayer simulation.

4.5. Order parameter

The presence of the peptide reduced the order parameters of the sn1 fatty acid chains of the lipids, which are spatially closer to the lipid head groups. However, except for the methylene closest to the head group, there was no influence on the order parameters of the sn2 chain (Fig. 13). We are not sure why the sn2 chain order parameters are affected by the presence of the peptide while the sn1 chain order parameters are not. Overall, there was no significant overall difference in the order parameters in the two simulations, especially near the core of the bilayer. These observations are in good agreement with NMR data, where the peptide was not seen to cause orientational disorder in shorter chain lipids [2].

5. Discussion

Yamaguchi's estimates of the tilt angles were considered accurate despite using solution structures of PG-1 to do the calculation. The reason was the high likelihood that the structure of PG-1 would be similar in solution and in membranes because it is stabilized by two disulfide bonds. The simulations show that most of the peptide has a similar structure in the DLPC bilayer as in solution. The backbone length of the peptide was the same in the simulation and the solution structure. However, the hydrophobic environment of the lipid bilayer induced a previously unseen "kick" shaped conformation of the C-terminal peptide region. The kick shaped conformation arose from a novel H-bond between the side chain of TYR7 and the GLY17 backbone (Fig. 8). The highly persistent H-bond relieves the unfavorable free energy of insertion of the polar hydroxyl group into the hydrophobic core of the bilayer. ARG4 formed a H-bond with the CYS15 backbone in CONF1, but in the CONF2 simulation, the ARG4 side chain was able to snorkel out towards the head groups. Conventional wisdom dictates that the residues localized in the transmembrane regions of peptides and protein

segments are mostly hydrophobic. However, there are several cases where polar amino acids side chains have been found to be localized in the hydrophobic membrane core. The two instances of backbone-sidechain H-bonds described here are examples of how bilayer-inserted polar side chains of a transmembrane peptide/protein segment forms H-bonds with the peptide backbone itself to offset the unfavorable free energy of insertion of both the polar side chains and the polar atoms on the peptide backbone. In the current work, such H-bonding leads to a subtle change in peptide structure: a C-terminal bend formed by residues 16–18 of the peptide, such that near the C-terminus, the peptide backbone is perpendicular to the overall plane of the peptide.

It is particularly difficult using experiments, such as solid state NMR, to estimate the orientation of β-hairpin structures in membranes because unlike helices, the backbone N—H bonds in β-hairpins are perpendicular to the principal axis of the β-sheet rather than parallel to it. Thus, a transmembrane peptide and an in-plane peptide would be indistinguishable in terms of their solid state ^{15}N spectra because the N—H bond will be perpendicular to the magnetic field in either case [2]. The current article demonstrates that MD simulations can be successfully used to accurately predict the orientation and conformation of β-sheet peptides in membranes.

It is not entirely clear why the PG-1 peptide adopts a tilted orientation in the DLPC lipid bilayer. The phosphate-to-phosphate thickness (D_p) of the DLPC bilayer is nearly 29.5± 0.27 Å in the peptide-bilayer simulation. The hydrophobic thickness of the bilayer ($2D_c$) is 20±0.24 Å. The average end to end length (L_e) of the PG-1 peptide backbone is about 25.9± 0.67 Å in the simulation, while the hydrophobic length of the backbone (residues 5–8 and 12–16) is 14.75±0.42 Å. If the peptide was parallel to the bilayer normal, the arginine-rich turn and termini region *backbone* of the peptide would be about 1.8 Å away from the average position of the phosphate groups of the lipids, while the hydrophobic region of the peptide would be inserted in the membrane core. Thus, based on a comparison of the end-to-end length of the peptide backbone and the bilayer thickness, there is apparently no significant hydrophobic mismatch which may cause the peptide to tilt, or the bilayer to thin. However, in the parallel orientation of the peptide, the arginine side chains may not be optimally positioned to bind to the anionic phosphate groups. The guanidium ion of an arginine residue can be as distant as 6–8 Å from the backbone owing to the long side chain. In the tilted orientation of the peptide, the projection of the peptide length along the bilayer normal is about 16–20 Å. In this orientation, the guanidium cations can "snorkel" [46] out into the interface and bind the phosphate anions. Furthermore, arginine is an amphipathic amino acid. In the tilted orientation, the hydrophobic methylene groups of the arginine side chains interact with the lipid fatty acid methylene groups close to the interface. It may be argued that if the peptide backbone is oriented parallel to the bilayer normal, the hydrophobic methylene groups on the arginine side chains will be spatially close to the charged regions of the lipid head groups, which may be energetically unfavorable.

Despite the small area of the bilayer simulated in the current work (~4300 Å^2), significant thinning of the bilayer near the peptide was observed. The local thinning near the peptide was approximately 6 Å, and it preserved the hydrophobic match between the hydrophobic core of the bilayer and the hydrophobic core region (residues 5–16) of the peptide. We think that the bilayer thinning is the result of two factors: the N-terminal anchor and the kick shaped conformation.

5.1. N-terminal anchor

The most significant peptide–lipid interaction to affect the orientation and position of the peptide in the bilayer was between the protonated N-terminus and the phosphate anions of the choline head group. The N-terminus anchored the peptide to the lower bilayer leaflet, resulting in the asymmetrical distribution of the peptide along the bilayer normal for the CONF1 simulation. This asymmetric location of the peptide in the two leaflets resulted in the turn-region arginine residues being closer to the core of the bilayer than the N-terminal and C-terminal arginine residues (Fig. 10). The electrostatic attraction of the lipid phosphate groups to the turn-region arginine residues (ARG9, ARG10, and ARG11) resulted in pulling of the lipid head groups towards the bilayer center, causing local thinning of the upper leaflet of the bilayer. The hypothesis is strengthened by the CONF1 simulation, where although ARG9, ARG10 and ARG11 were bound to the phosphate head groups as strongly as in CONF2, the bilayer thinning was insignificant because these residues were close to the head group region.

6.2. Kick-conformation

The "kick" conformation of the peptide sampled in the CONF2 simulation caused the C-terminus of the peptide to move away from the head group region towards the bilayer core. However, ARG18 was still bound strongly to the lipid head groups, which therefore got pulled towards the bilayer center, resulting in thinning in the lower leaflet of the bilayer. In the CONF1 simulation, there was no kick-shaped conformation, and hence ARG18 was near the head group region, and did not cause bilayer thinning despite binding strongly to the phosphate head groups.

The "kick" conformation of the peptide, which was sampled in the CONF1 simulation, was not sampled in the CONF2 simulation, where the peptide was initially placed at a 45 degree angle to the bilayer normal. In the CONF2 simulation, the TYR7–GLY17 H-bond was not detected, and both peptide termini had an extended backbone. Although the final conformation of the C-terminus of the peptide is different in the two simulations, the equilibrium orientation of the peptide w.r.t. the bilayer is the same in either case, and is very similar to the orientation predicted by NMR experiments. Based on the convergence of the peptide orientation in both the simulations, it may be argued that PG-1 may adopt at least two different, stable equilibrium conformations in the DLPC lipid bilayer. It is also possible that one of the two main conformations observed in the simulations is a local minimum on the energy landscape, but

there is no clear way to identify which one. The energy of the CONF1 and CONF2 simulations over the ensemble averaged period were −50698.11±67.48 and −50688.15±72.8 kcal/mole. The energy of the CONF1 conformation is 10 kcal/mole lower than that of the CONF2 conformations, and it may be the more stable conformation. However, 10 kcal/mole is not a significantly large difference, and is within the amplitude of the energy fluctuations. It is more likely that the equilibrium structure of the peptide fluctuates between the two conformations, because both conformations yield an identical orientation in the membrane, which is seen in experiments. Either way, it is clear that the initial orientation of the peptide in the simulations has a bearing on which conformations of the peptide in phase space are accessible to each simulation, and this dependence of the simulation results on the initial simulation setup emphasizes the importance of starting simulations with adequately different initial configurations to sample the maximum possible peptide conformations. There is no certainty that the peptide conformations sampled in the CONF2 simulation will become accessible to the CONF1 simulation by extending the length of the CONF1 simulation (or vice versa).

The current work provides a rich molecular description of the interaction of PG-1 with a zwitterionic lipid bilayer, the influence of the lipid bilayer on peptide structure, and vice versa. To obtain further insight into the mechanism of pore formation by PG-1, multiple peptides in lipid bilayers of varying compositions (longer chain lipids, charged lipids) need to be investigated. Oligomerization of PG-1 in lipid bilayers is now identified as a critical step towards membrane lysis [20,22,28]. Further simulations are also necessary to address the selectivity of PG-1 towards anionic lipids in preference to zwitterionic lipids like DLPC. These investigations are currently underway.

Acknowledgements

We thank Prof. Alan Waring and Prof. Mei Hong for useful discussions. This work was supported by grants from NSF (EEC-0234112) and NIH (GM 070989). Computational support from the Minnesota Supercomputing Institute (MSI) is gratefully acknowledged. This work was also partially supported by National Computational Science Alliance under MCB030027P and utilized the marvel cluster at the Pittsburgh Supercomputing Center, and the tungsten cluster at the NCSA.

References

[1] R.L. Fahrner, T. Dieckmann, S.S.L. Harwig, R.I. Lehrer, D. Eisenberg, J. Feigon, Solution structure of protegrin-1, a broad-spectrum antimicrobial peptide from porcine leukocytes, Chem. Biol. 3 (1996) 543–550.

[2] S. Yamaguchi, T. Hong, A. Waring, R.I. Lehrer, M. Hong, Solid-state NMR investigations of peptide–lipid interaction and orientation of a b-sheet antimicrobial peptide, protegrin, Biochemistry 41 (2002) 9852–9862.

[3] M. Zasloff, Antimicrobial peptides of multicellular organisms, Nature 415 (2002) 389–395.

[4] V. Morell, Antibiotic resistance: road of no return, Science 278 (1997) 575–576.

[5] V.N. Kokryakov, S.S. Harwig, E.A. Panyutich, A.A. Shevchenko, G.M. Aleshina, O.V. Shamova, H.A. Korneva, R.I. Lehrer, Protegrins: leukocyte antimicrobial peptides that combine features of corticostatic defensins and tachyplesins, FEBS Lett. 327 (1993) 231–236.

[6] D.A. Steinberg, M.A. Hurst, C.A. Fukii, A.H.C. Kung, J.F. Ho, F.C. Cheng, D.J. Loury, J.C. Fiddes, Protegrin-1: a broad-spectrum, rapidly microbicidal peptide with in vivo activity, Antimicrob. Agents Chemother. 41 (1997) 1738–1742.

[7] W.T. Heller, A.J. Waring, R.I. Lehrer, T.A. Harroun, T.M. Weiss, L. Yang, H.W. Huang, Membrane thinning effect of the b-sheet Antimicrobial Protegrin, Biochemistry 39 (2000) 139–145.

[8] Y. Sokolov, T. Mirzabekov, D.W. Martin, R.I. Lehrer, B.L. Kagan, Membrane channel formation by antimicrobial protegrins, Biochim. Biophys. Acta 1420 (1999) 23–29.

[9] L. Yang, T.M. Weiss, R.I. Lehrer, H.W. Huang, Crystallization of antimicrobial pores in membranes: magainin and protegrin, Biophys. J. 79 (2000) 2002–2009.

[10] D. Gidalevitz, Y. Ishitsuka, A.S. Muresan, O. Konovalov, A.J. Waring, R.I. Lehrer, K.Y.C. Lee, Interaction of antimicrobial peptide protegrin with biomembranes, Proc. Natl. Acad. Sci. U. S. A. 100 (2003) 6302–6307.

[11] M.E. Mangoni, A. Aumelas, P. Charnet, C. Roumestand, L. Chiche, E. Despaux, G. Grassy, B. Calas, A. Chavanieu, Change in membrane permeability induced by protegrin 1: implication of disulfide bridges for pore formation, FEBS Lett. 383 (1996) 93–98.

[12] A. Aumelas, M. Mangoni, C. Roumestand, L. Chiche, E. Despaux, G. Grassy, B. Calas, A. Chavanieu, Synthesis and solution structure of the antimicrobial peptide protegrin-1, Eur. J. Biochem. 237 (1996) 575–583.

[13] S.S. Harwig, A. Waring, H.J. Yang, Y. Cho, L. Tan, R.I. Lehrer, Intramolecular disulfide bonds enhance the antimicrobial and lytic activities of protegrins at physiological sodium chloride concentrations, Eur. J. Biochem. 240 (1996) 352–357.

[14] J. Chen, T.J. Falla, H. Liu, M.A. Hurst, C.A. Fujii, D.A. Mosca, J.R. Embree, D.J. Loury, P.A. Radel, C.C. Chang, L. Gu, J.C. Fiddes, Development of protegrins for the treatment and prevention of oral mucositis: structure–activity relationships of synthetic protegrin analogues, Biopolymers 55 (2000) 88–98.

[15] D.A. Devine, Antimicrobial peptides in defence of the oral and respiratory tracts, Mol. Immunol. 40 (2003) 431–443.

[16] J.H. Toney, Iseganan (IntraBiotics Pharmaceuticals), Curr. Opin. Investig. Drugs 3 (2002) 225–228 (PharmaPress Ltd.).

[17] Y.J. Gordon, E.G. Romanowski, A.M. McDermott, A review of antimicrobial peptides and their therapeutic potential as anti-infective drugs, Curr. Eye Re. 30 (2005) 505–515.

[18] W.T. Heller, A.J. Waring, R.I. Lehrer, H.W. Huang, Multiple states of beta-sheet peptide protegrin in lipid bilayers, Biochemistry 37 (1998) 17331–17338.

[19] G. Drin, J. Temsamani, Translocation of protegrin I through phospholipid membranes: role of peptide folding, Biochim. Biophys. Acta 1559 (2002) 160–170.

[20] J.J. Buffy, A.J. Waring, M. Hong, Determination of peptide oligomerization in lipid bilayers using 19F spin diffusion NMR, J. Am. Chem. Soc. 127 (2005) 4477–4483.

[21] J.J. Buffy, T. Hong, S. Yamaguchi, A.J. Waring, R.I. Lehrer, M. Hong, Solid-state NMR investigation of the depth of insertion of protegrin-1 in lipid bilayers using paramagnetic Mn2+, Biophys. J. 85 (2003) 2363–2373.

[22] J.J. Buffy, A.J. Waring, R.I. Lehrer, M. Hong, Immobilization and aggregation of the antimicrobial peptide protegrin-1 in lipid bilayers investigated by solid-state NMR, Biochemistry 42 (2003) 13725–13734.

[23] R. Mani, J.J. Buffy, A.J. Waring, R.I. Lehrer, M. Hong, Solid-state NMR investigation of the selective disruption of lipid membranes by protegrin-1, Biochemistry 43 (2004) 13839–13848.

[24] R. Mani, A.J. Waring, R.I. Lehrer, M. Hong, Membrane-disruptive abilities of beta-hairpin antimicrobial peptides correlate with conformation and activity: a 31P and 1H NMR study Biochim, Biophys. Acta 1716 (2005) 11–18.

[25] P.A.B. Marasinghe, J.J. Buffy, K. Schmidt-Rohr, M. Hong, Membrane curvature change induced by an antimicrobial peptide detected by 31P exchange NMR, J. Phys. Chem., B 109 (2005) 22036–22044.

[26] W. Jing, E.J. Prenner, H.J. Vogel, A.J. Waring, R.I. Lehrer, K. Lohner, Headgroup structure and fatty acid chain length of the acidic phospholipids modulate the interaction of membrane mimetic vesicles with the antimicrobial peptide protegrin-1, J. Pept. Sci. 11 (2005) 735–743.
[27] M. Tang, A.J. Waring, M. Hong, Intermolecular packing and alignment in an ordered b-hairpin antimicrobial peptide aggregate from 2D solid-state NMR, J. Am. Chem. Soc. 127 (2005) 13919–13927.
[28] R. Mani, M. Tang, X. Wu, J.J. Buffy, A.J. Waring, M.A. Sherman, M. Hong, Membrane-bound dimer structure of a beta-hairpin antimicrobial peptide from rotational-echo double-resonance solid-state NMR, Biochemistry 45 (2006) 8341–8349.
[29] A. Aumelas, M. Mangoni, C. Roumestand, L. Chiche, E. Despaux, G. Grassay, B. Calas, A. Chavenieu, Synthesis and solution structure of the antimicrobial peptide protegrin-1, Eur. J. Biochem. 237 (1996) 575–583.
[30] B. Roux, Commentary: surface tension of biomembranes, Biophys. J. 71 (1996) 1346–1347.
[31] S.E. Feller, R.W. Pastor, On simulating lipid bilayers with an applied surface tension: periodic boundary conditions and undulations, Biophys. J. 71 (1996) 1350–1355.
[32] F. Jaehnig, What is the surface tension of a lipid bilayer membrane? Biophys. J. 71 (1996) 1348–1349.
[33] M.O. Jensen, O.G. Mouritsen, G.H. Peters, Simulations of a membrane-anchored peptide: structure, dynamics, and influence on bilayer properties, Biophys. J. 86 (2004) 3556–3575.
[34] B.R. Brooks, R.E. Bruccoleri, B.D. Olfson, D.J. States, S. Swaminathan, K. Karplus, CHARMM: a program for macromolecular energy, minimization, and dynamics calculations, J. Comput. Chem. 4 (1983) 187–217.
[35] S.E. Feller, R.W. Pastor, Constant surface tension simulations of lipid bilayers: the sensitivity of surface areas and compressibilities, J. Chem. Phys. 111 (1999) 1281–1287.
[36] Y.H. Zhang, S.E. Feller, B.R. Brooks, R.W. Pastor, Computer-simulation of liquid/liquid interfaces: 1. Theory and application to octane/water, J. Chem. Phys. 103 (1995) 10252–10266.
[37] T.B. Woolf, B. Roux, in: K. Merz, B. Roux (Eds.), Biological Membranes: A Molecular Perspective from Computation and Experiment, Birkhauser, Boston, 1996, pp. 555–587.
[38] W.L. Jorgensen, J. Chandrasekhar, J.D. Medura, M.L. Klein, Comparison of simple potential function for simulating liquid water, J. Chem. Phys. 79 (1983) 926–935.
[39] N. Kucerka, Y. Liu, N. Chu, H.I. Petrache, S. Tristram-Nagle, J.F. Nagle, Structure of fully hydrated fluid phase DMPC and DLPC lipid bilayers using X-ray scattering from oriented multilamellar arrays and from unilamellar vesicles, Biophys. J. 88 (2005) 2626–2637.
[40] P. Balgavy, M. Dubnickova, N. Kucerka, M.A. Kiselev, S.P. Yaradaikin, D. Uhrikova, Bilayer thickness and lipid interface area in unilamellar extruded 1,2-diacylphosphatidylcholine liposomes: a small-angle neutron scattering study Biochim, Biophys. Acta 1512 (2001) 40–52.
[41] B.A. Lewis, D.M. Engelman, Lipid bilayer thickness varies linearly with acyl chain length in fluid phosphatidylcholine vesicles, J. Mol. Biol. 166 (1983) 211–217.
[42] W.G. Hoover, Canonical dynamics: equilibrium phase-space distributions, Phys. Rev., A 31 (1985) 1695–1697.
[43] S.E. Feller, Y. Zhang, R.W. Pastor, B.R. Brooks, Constant pressure molecular dynamics simulation: the Langevin piston method, J. Chem. Phys. 103 (1995) 4613–4621.
[44] U. Essmann, L. Perera, M.L. Berkowitz, T. Darden, H. Lee, L.G. Pedersen, A smooth particle mesh Ewald method, J. Chem. Phys. 103 (1995) 8577–8593.
[45] T.P. Trouard, A.A. Nevzorov, T.M. Alam, C. Job, J. Zajicek, M.F. Brown, Influence of cholesterol on dynamics of dimyristoylphosphatidylcholine bilayers as studied by deuterium NMR relaxation, J. Chem. Phys. 110 (1999) 8802–8818.
[46] I. Zelezetsky, S. Pacor, U. Pag, N. Papo, Y. Shai, H.G. Sahl, A. Tossi, Controlled alteration of the shape and conformational stability of alpha-helical cell-lytic peptides: effect on mode of action and cell specificity, Biochem. J. 390 (2005) 177–188.